JOURNAL OF APPLIED ELECTROCHEMISTRY 7 (1977) 287–297.

A thermodynamic estimation of the minimum concentration attainable in a flow-through porous electrode reactor

J. A. TRAINHAM, J. NEWMAN

Materials and Molecular Research Div., Lawrence Berkeley Laboratory and Department of Chemical Engineering, University of California, Berkeley, California 94720, USA

Received 29 July 1976

The minimum concentration attainable in a porous flow-through reactor is estimated by applying the thermodynamics of electrochemical cells with a knowledge of the maximum reactor operating potential. This predicted concentration is the equilibrium wall concentration at the back of the reactor and is qualitatively compared to the experimentally measured minimum average bulk values observed by various authors for the deposition of copper, silver, lead, and mercury, and for the oxidation of ferrous ions. It is suggested that a knowledge of the current versus reactor operating potential will elucidate the lower limits observed for any metal system. In particular, the case of antimony removal is discussed.

Notation

a	specific interfacial area, cm^{-1}
a_i^θ	$= \lambda_i^\theta/\rho_o$ property expressing the secondary reference state, $l\ mol^{-1}$
c_i	molar concentration of species i, $mol\ l^{-1}$
$c_{Cl^-,\,sat}$	concentration of chloride ion in a saturated calomel reference electrode compartment
c_f	feed concentration to porous electrode, $mol\ cm^{-3}$
f_i	molar activity coefficient of species i
$f_{i,n}$	$= f_i/f_n^{z_i/z_n}$ molar activity coefficient of species i referred to the ionic species n
F	Faraday's constant, 96 487 C $equiv^{-1}$.
i	superficial current density to porous electrode, $A\ cm^{-2}$
k_m	coefficient of mass transfer between flowing solution and electrode surface, $cm\ s^{-1}$
n	number of electrons involved in electrode reaction
R	universal gas constant, 8·3143 J ($mol\text{-}deg^{-1}$)
T	absolute temperature, deg K
U	open-circuit cell potential, V
U_k^θ	standard electrode potential for electrode reaction k, V
v	superficial velocity, $cm\ s^{-1}$
VOP	potential of the cathode current collector relative to a given reference electrode placed in the dilute product stream, V
$(VOP)_{max}$	maximum value of VOP at which appreciable side reaction does not occur, V
ΔV_k	$VOP - U_k^\theta + U_{cal}^\theta$

Greek letters

β_ϵ	overall stability constant, where ϵ denotes the number of ligands in the complex, $(l\ mol^{-1})^\epsilon$ or $(kg\ mol^{-1})^\epsilon$
κ	effective conductivity of solution, $mho\ cm^{-1}$
λ_i	absolute activity of species i
λ_i^θ	property expressing secondary reference state, $kg\ mol^{-1}$
$\lambda_{i,n}^\theta$	$= \lambda_i^\theta/\lambda_n^{\theta\, z_i/z_n}$ property expressing secondary reference state of species i referred to ionic species n

σ	effective conductivity of matrix, mho cm^{-1}
μ_i	electrochemical potential of species i, $J\,mol^{-1}$
ρ_o	density of pure solvent, $g\,cm^{-3}$
Φ	quasi-electrostatic potential, V
Φ_1	matrix potential, V
Φ_2	solution potential, V
$\Delta\Phi_2'$	estimate of allowable ohmic drop across a porous flow-through electrode reactor operating at the limiting current, V

Superscripts

o	pure state
θ	secondary reference state at infinite dilution
*	ideal-gas secondary reference state

Subscripts

f	feed
sat	saturated
cal	calomel

1. Introduction

The removal of heavy metals from industrial wastes by porous flow-through electrode reactors is promising, although not yet proved to be technologically and economically feasible. Encouraging results have been obtained in studies [1–3] on the removal of various metals and in comparisons [4, 5] to other electrochemical reactors.

On the other hand, there are results which are less encouraging. In the removal of lead ions the authors [6] have had difficulty in reducing the effluent concentration below 0·5 mg l^{-1}. In the work of Kuhn and Houghton [7], the concentration of antimony was reduced from 100 mg l^{-1} in the feed to a dilute product concentration not lower than 5 mg l^{-1}. This apparent limit was explained as being the equilibrium concentration at which deposition and dissolution of antimony occurs at the same rate.

The purpose of this paper is to suggest a criterion by which one may estimate the minimum attainable dilute product concentration given the maximum operating potential, or given a desired dilute product concentration the minimum value of the operating potential at which this dilute product concentration can be achieved, thus providing a basis for design and operation.

In the design of electrochemical reactors, it is desirable to avoid side reactions. Such reactions occur if the potential variation in the solution exceeds a certain limit. Since a characteristic of porous flow-through electrode reactors is the non-uniform ohmic potential drop, the operating potential may not be set arbitrarily high. The maximum operating potential is that potential which may be maintained in the reactor at which an appreciable side reaction does not occur. This can be determined experimentally by measuring the current versus the potential of the working electrode current collector relative to a given reference electrode placed in the effluent stream (*VOP*, shown schematically in Fig. 1). *VOP* as shown in Fig. 1 is the potential difference $\Phi_{met} - \Phi_{soln}$, where Φ_{met} is the electrostatic potential of the constant potential current collector and Φ_{soln} is the quasi-electrostatic potential [8a] of the solution leaving the reactor.

Various authors [1, 2, 6, 9] have used the configuration shown in Fig. 1 to obtain the current–potential behaviour of these reactors. Inspection of the resulting current–potential curve yields a value of the maximum operating potential VOP_{max}. If it is assumed that the reactant species leaving the reactor is in equilibrium with the working electrode current collector at the potential VOP_{max}, a value of the lower limit of removal of the reactant species may be calculated.

In order to attain a low effluent concentration, we envisage placement of the counter-electrode upstream of the working electrode in Fig. 1. This results in the potential distribution shown in Fig. 2 (see [10] for details). The current flowing in the solution drops to zero at the back of the electrode and, because the reaction rate is also low in this region, the potential variation in the solution may also be small over a considerable portion of the thickness of the electrode. In this region, the potential difference between the matrix and the solution will be approximately equal to VOP ($-\Phi_{2L}$ in Fig. 2), and thus there may be some substantial distance over which the bulk concentration can be approaching the wall concentration.

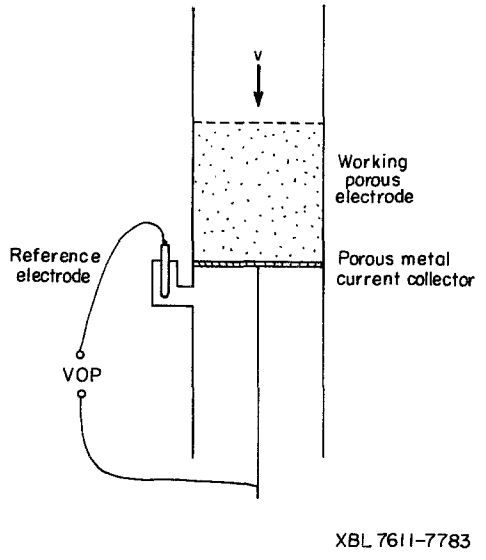

Fig. 1. Measurement of *VOP* in a flow-through porous electrode.

An alternative electrode configuration [11, 12] involves placement of the counter-electrode adjacent to the working electrode, so that the fluid flow is parallel to the separation between the electrodes. (A similar configuration has been used where the electrodes are fluidized beds [13] rather than packed beds.) In order to attain a low effluent concentration, the electrodes are then made long in the direction of flow. Since the reaction rate decreases in the downstream region, there will again be a substantial distance where the potential difference between the matrix and the solution will be approximately equal to *VOP*.

An undesirable configuration, from the point of view of attaining a low effluent concentration, is where the counter-electrode is placed downstream and the current collector upstream in Fig. 1. The corresponding potential distribution in the solution is also shown in Fig. 2 (see [10] for details) as a dashed curve and is drawn for the same total current as the curve for the upstream counter-electrode (for these calculated potential distributions the effluent concentration is less by a factor of 61 for the upstream placement of the counter-electrode than for the downstream placement of the counter-electrode). In contrast to the two configurations discussed above, the solution potential varies substantially in the downstream region, because the current here is the total current flowing to the counter-electrode, and an

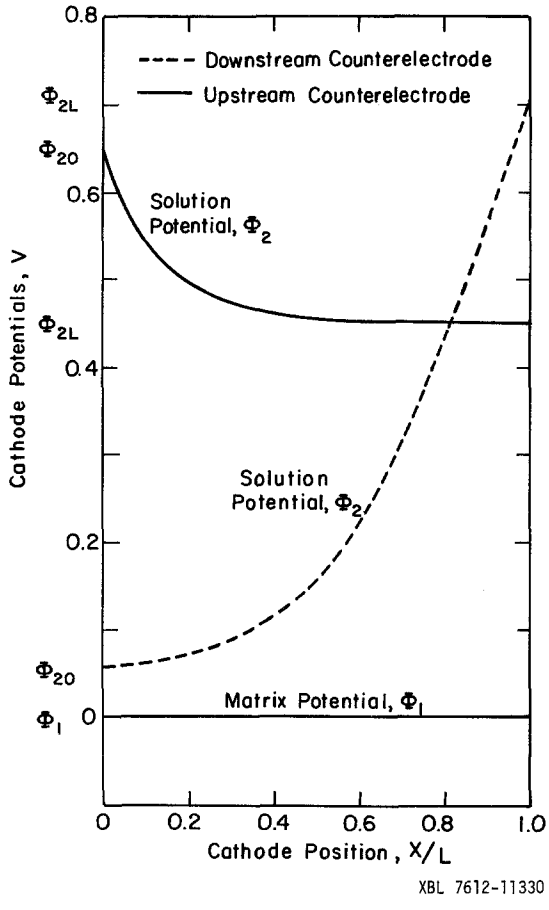

Fig. 2. Calculated [10] solution-phase and solid-matrix-phase potential distributions for the deposition of copper and simultaneous formation of dissolved hydrogen for the following cases: (1) downstream placement of the counter-electrode with a downstream current collector, where the matrix conductivity σ is considerably greater than the solution conductivity κ. Φ_2 is the potential measured with a copper reference electrode with $c_{Cu^{2+}} = c_f$ in the reference electrode compartment. The calculations in both cases were done for $v = 3{\cdot}328 \times 10^{-3}$ cm s^{-1}, $c_f = 1{\cdot}05 \times 10^{-5}$ mol cm^{-3}, $a = 25$ cm^{-1}, $i = -0{\cdot}007$ A cm^{-2}, and $L = 6$ cm.

increase of the electrode dimension in the direction of fluid flow will not necessarily have a beneficial effect on the removal or recovery of the solute. The maximum electric driving force $(\Phi_1 - \Phi_2)$ occurs at the downstream end of the electrode, but this does not prevail over a substantial distance. If this maximum electric driving force is restricted so that undesirable side reactions are maintained at a tolerable level, then only a greatly diminished electric driving force will be available over much of the electrode thickness,

and the effluent concentration cannot be expected to drop to the thermodynamic value corresponding to the measured value of VOP ($-\Phi_{2L}$ in Fig. 2).

In the applications of this work, we think in terms of the first two configurations, where the potential difference between the matrix and the solution can be made approximately equal to VOP over a considerable distance. Also in a recycle system [7] or a system with several reactors in series, it is possible to allow adequate opportunity for the effluent concentration to approach the thermodynamic value corresponding to a given value of VOP.

2. Analysis

In order to calculate the minimum attainable concentration in a porous flow-through electrode reactor, using the values of VOP_{max}, one can mentally construct an electrochemical cell which consists of the working electrode and the given reference electrode. An expression for the open-circuit cell potential U may then be derived using thermodynamics if the following assumptions are made:

(1) The reactor has been run sufficiently long that metal deposition of the reactant has occurred.

(2) Equilibrium exists between the reacting species and the deposited metal.

(3) The molecular and ionic forms of the reacting species are known.

The value of VOP_{max} is then substituted for U, and the equilibrium wall concentration for a particular reacting species is obtained. The total equilibrium wall concentration is simply the sum of all the reacting species which are in equilibrium with the deposited metal. This calculated value will be lower than the actual effluent concentration because of a lack of equilibrium at the downstream end of the reactor due to a non-zero reaction rate and electrode kinetic and mass-transfer limitations.

The following examples will help to clarify the method.

2.1. *Copper deposition from sulphate solutions*

Bennion and Newman [1] have obtained the current–potential behaviour of a porous carbon reactor used in the removal of copper from sulphate solutions. From their data, a value of VOP_{max} equal to $-0{\cdot}25$ V may be chosen. A schematic representation of this cell is as follows:

α	β	δ	ϵ		δ'	ϕ	α'
Pt(s)	Hg(l)	Hg_2Cl_2(s)	KCl saturated in H_2O	transition region	$CuSO_4$ in H_2SO_4 and H_2O	Cu(s)	Pt(s)

where the reaction at the left electrode is

$$2Hg + 2Cl^- \rightleftarrows Hg_2Cl_2 + 2e^-, \qquad (1)$$

and one possible reaction at the right electrode is

$$Cu^{2+} + 2e^- \rightleftarrows Cu. \qquad (2)$$

An expression for the open-circuit cell potential U may be derived using the thermodynamics of electrochemical cells, for example, see Newman [8a]. For this cell, the open-circuit cell potential was found to be

$$FU = FU^\theta + \tfrac{1}{2}RT \ln \frac{c_{Cu^{2+}} c^2_{Cl^-,sat}}{\rho_o^3} + \tfrac{1}{2}RT \ln f_{Cu^{2+},Cl^-} + F(\Phi^\delta - \Phi^{\delta'}), \qquad (3)$$

where

$$FU^\theta = \mu^\circ_{Hg} - \tfrac{1}{2}\mu^\circ_{Cu} - \tfrac{1}{2}\mu^\circ_{Hg_2Cl_2} + \tfrac{1}{2}RT \ln \lambda^\theta_{Cu^{2+},Cl^-}. \qquad (4)$$

Thus, the value of the standard cell potential for this cell at 25° C is

$$U^\theta = 0{\cdot}337 - 0{\cdot}2676 = 0{\cdot}0694\,\text{V}.$$

Omission of the activity coefficient and liquid junction potential terms (the fourth and fifth terms) in Equation 3 will result in a satisfactory estimate of the equilibrium copper concentration. With these considerations Equation 3 may be rearranged to yield an expression for the equilibrium cupric concentration as follows:

$$c_{Cu^{2+}} = \frac{\rho_o^3}{c^2_{Cl^-,sat}} \exp\left(\frac{2F}{RT}\Delta V_k\right) = 9{\cdot}07 \times 10^{-13}\ \text{mol l}^{-1} \qquad (5)$$

where U has been set equal to VOP_{max}, $\Delta V_k =$

$VOP_{max} - U^{\theta}$, and $c_{Cl^-,sat} = 4{\cdot}17\ mol\ l^{-1}$.

As was mentioned previously, the deposition of copper from cupric ions is not the only equilibrium electrode process. Cuprous ions are also in equilibrium with both the deposited copper and the cupric ions. The equilibrium cuprous concentration can be calculated as was done earlier for the cupric ions. However, cuprous ions disproportionate according to

$$2Cu^+ \rightleftarrows Cu + Cu^{2+}. \quad (6)$$

The equilibrium constant for this reaction is [8b]

$$\frac{c^2_{Cu^+} f^2_{Cu^+}}{c_{Cu^{2+}} f_{Cu^{2+}} \rho_o} = \frac{1}{1{\cdot}67 \times 10^6}\ mol\ kg^{-1}. \quad (7)$$

With neglect of activity coefficients the equilibrium cuprous concentration is found to be:

$$c_{Cu^+} = (c_{Cu^{2+}} \rho_o / 1{\cdot}67 \times 10^6\ kg\ mol^{-1})^{1/2} = 7{\cdot}359 \times 10^{-10}\ mol\ l^{-1}. \quad (8)$$

Therefore the total equilibrium copper concentration is

$$(c_{Cu})_{total} = c_{Cu^{2+}} + c_{Cu^+} = 7{\cdot}37 \times 10^{-10}\ mol\ l^{-1}$$

or $4{\cdot}68 \times 10^{-5}\ mg\ l^{-1}$.

2.2. *Silver deposition from photographic fixing solutions*

Van Zee and Newman [2] have obtained the current–potential behaviour of a porous carbon reactor used for removing silver from photographic fixing solutions. From their data, a value of $VOP_{max} = -0{\cdot}46$ V was chosen due to appreciable side reaction, thought to be

$$S_2O_3^{2-} + 8e^- + 8H^+ \rightarrow 2HS^- + 3H_2O, \quad (9)$$

which occurs at a significant rate for more extreme values of *VOP*. Silver ions in solutions containing thiosulphate form a very stable complex [14]:

$$Ag^+ + 2S_2O_3^{2-} \rightleftarrows Ag(S_2O_3)_2^{3-}, \quad (10)$$

which has a value of the stability constant β_2 of approximately [14]:

$$\beta_2 = \frac{f_{Ag(S_2O_3)_2^{3-}}\, c_{Ag(S_2O_3)_2^{3-}}\, \rho_o^2}{f_{Ag^+}\, c_{Ag^+} (f_{S_2O_3^{2-}}\, c_{S_2O_3^{2-}})^2} = \frac{\lambda^{\theta}_{Ag^+} (\lambda^{\theta}_{S_2O_3^{2-}})^2}{\lambda^{\theta}_{Ag(S_2O_3)_2^{3-}}} = 1{\cdot}7 \times 10^{13}\ (kg\ mol^{-1})^2. \quad (11)$$

Therefore, it will be necessary to consider the deposition of silver from the silver-thiosulphate complex:

$$Ag + 2S_2O_3^{2-} \rightleftarrows Ag(S_2O_3)_2^{3-} + e^-, \quad (12)$$

which has an expression for the standard electrode potential

$$FU^{\theta}_{Ag/Af(S_2O_3)_2^{3-}} = \tfrac{1}{2}\mu^*_{H_2} - \mu^o_{Ag} - 2RT \ln \lambda^{\theta}_{S_2O_3^{2-}} + RT \ln \lambda^{\theta}_{Ag(S_2O_3)_2^{3-}}/\lambda^{\theta}_{H^+}. \quad (13)$$

The value for $U^{\theta}_{Ag/Ag(S_2O_3)_2^{3-}}$ may be calculated from the value of the stability constant of the species $Ag(S_2O_3)_2^{3-}$ and the standard electrode potential of the non-complexed silver deposition reaction:

$$Ag \rightleftarrows Ag^+ + e^-. \quad (14)$$

The expression for the standard electrode potential is

$$FU^{\theta}_{Ag/Ag^+} = \tfrac{1}{2}\mu^*_{H_2} - \mu^o_{Ag} + RT \ln \lambda^{\theta}_{Ag^+}/\lambda^{\theta}_{H^+} \quad (15)$$

where $U^{\theta}_{Ag/Ag^+} = 0{\cdot}7991$ V. Equations 13 and 15 lead to

$$U^{\theta}_{Ag/Ag(S_2O_3)_2^{3-}} = U^{\theta}_{Ag/Ag^+} - \frac{RT}{F} \ln \beta_2 = 0{\cdot}0164\ V, \quad (16)$$

which indicates that silver will be much more difficult to plate in the presence of thiosulphate ions due to hydrogen evolution.

A schematic diagram of the electrochemical cell which consists of a silver–silver thiosulphate electrode and the calomel reference electrode is as follows:

α	β	δ	ϵ			δ'	ϕ	α'
Pt(*s*)	Hg(*l*)	Hg_2Cl_2(*s*)	KCl saturated in H_2O	transition region		$Ag(S_2O_3)_2^{3-}$ in $Na_2S_2O_3 \cdot 5H_2O$, $NaHSO_3$, NaBr	Ag(*s*)	Pt(*s*)

An expression for the equilibrium $Ag(S_2O_3)_2^{3-}$ concentration as a function of *VOP* may be derived as was done previously for the copper system. This expression with neglect of activity

coefficients and the liquid junction potential is

$$c_{Ag(S_2O_3)_2^{3-}} = \frac{c^2_{S_2O_3^{2-}}}{c_{Cl^-,\,sat}} \exp\left(\frac{F}{RT}\Delta V_k\right), \quad (17)$$

where $\Delta V_k = VOP - U^\theta_{Ag/Ag(S_2O_3)_2^{3-}} + U^\theta_{cal}$. For $c_{S_2O_3^{2-}} = 1{\cdot}737\ \text{mol}\ l^{-1}$ and $VOP_{max} = -0{\cdot}46\ \text{V}$, the value of the equilibrium silver concentration is $2{\cdot}14 \times 10^{-4}\ \text{mol}\ l^{-1}$ or $23\ \text{mg}\ l^{-1}$ of silver.

2.3. *Mercury removal from brine solutions*

This example combines aspects of the previous two examples, i.e., multiple electrode reaction equilibria and complexing. Mercuric ions Hg^{2+} form very stable chloride complexes with stability constants of the form

$$\beta_\epsilon = \frac{f_{HgCl_\epsilon^{2-\epsilon}} c_{HgCl_\epsilon^{2-\epsilon}}}{f_{Hg^{2+}} c_{Hg^{2+}} (f_{Cl^-} c_{Cl^-})^\epsilon} = \frac{a^\theta_{Hg^{2+}} (a^\theta_{Cl^-})^\epsilon}{a^\theta_{HgCl_\epsilon^{2-\epsilon}}} \quad (18)$$

which have values: $\ln \beta_1 = 12{\cdot}2$, $\ln \beta_2 = 29{\cdot}4$, $\ln \beta_3 = 32{\cdot}0$, and $\ln \beta_4 = 34{\cdot}3$ [15]. The mercurous dimer Hg_2^{2+} does not complex appreciably in chloride solutions [16].

Table 1 lists the expressions and values for the standard electrode potentials of mercury. The standard electrode potentials involving the complexed species were calculated using the above stability constant data. For example, entries 6 and 8 were calculated from entries 2 and 1, respectively, using the value of β_4 as follows:

$$U^\theta_{Hg/HgCl_4^{2-}} = U^\theta_{Hg/Hg^{2+}} - \frac{RT}{2F} \ln \beta_4. \quad (19)$$

$$U^\theta_{Hg_2^{2+}/HgCl_4^{2-}} = U^\theta_{Hg_2^{2+}/Hg^{2+}} - \frac{RT}{F} \ln \beta_4. \quad (20)$$

Expressions for the equilibrium mercuric chloride complex concentrations as a function of *VOP* may be derived as in previous examples:

$$c_{HgCl_2} = \frac{c^2_{Cl^-} \rho_o}{c^2_{Cl^-,\,sat}} \exp\left(\frac{2F}{RT}\Delta V_k\right), \quad (21)$$

$$c_{HgCl_3^-} = \frac{c^3_{Cl^-}}{c^2_{Cl^-,\,sat}} \exp\left(\frac{2F}{RT}\Delta V_k\right), \quad (22)$$

$$c_{HgCl_4^{2-}} = \frac{c^4_{Cl^-}}{\rho_o c^2_{Cl^-,\,sat}} \exp\left(\frac{2F}{RT}\Delta V_k\right), \quad (23)$$

where ΔV_k refers to the electrode reaction involving the appropriate mercuric complex (activity coefficient corrections and the liquid junction potential were neglected).

The expressions for the species $HgCl^+$ and Hg^{2+} are not given since their contribution to the equilibrium mercury concentration is negligible in comparison with the highly complexed species. The equilibrium concentration of the mercurous dimer may be related to the mercuric chloride complex concentrations by the appropriate disproportionation reaction. For example, consider the reaction

$$Hg_2^{2+} + 3Cl^- \rightleftarrows Hg + HgCl_3^-, \quad (24)$$

with the result

$$c_{Hg_2^{2+}} = \frac{\rho_o^3 c_{HgCl_2^-}}{c^3_{Cl^-}} \times$$

Table 1. Standard electrode potentials of mercury referred to the hydrogen electrode. Aqueous solutions at 25° C

Reaction	FU^θ	U^θ (V)
(1) $Hg_2^{2+} \rightarrow 2Hg^{2+} + 2e^-$	$\frac{1}{2}\mu^*_{H_2} - \frac{1}{2}RT \ln \lambda^\theta_{Hg_2^{2+}} + RT \ln \lambda^\theta_{Hg^{2+}}/\lambda^\theta_{H^+}$	0·920
(2) $Hg \rightarrow Hg^{2+} + 2e^-$	$\frac{1}{2}\mu^*_{H_2} - \frac{1}{2}\mu^o_{Hg} + \frac{1}{2}RT \ln \lambda^\theta_{Hg^{2+}}/(\lambda^\theta_{H^+})^2$	0·854 5
(3) $2Hg \rightarrow Hg_2^{2+} + 2e^-$	$\frac{1}{2}\mu^*_{H_2} - \mu^o_{Hg} + \frac{1}{2}RT \ln \lambda^\theta_{Hg_2^{2+}}/(\lambda^\theta_{H^+})^2$	0·789
(4) $Hg + 2Cl^- \rightarrow HgCl_2 + 2e^-$	$\frac{1}{2}\mu^*_{H_2} - \frac{1}{2}\mu^o_{Hg} - RT \ln \lambda^\theta_{Cl^-} + \frac{1}{2}RT \ln \lambda^\theta_{HgCl_2}/(\lambda^\theta_{H^+})^2$	0·476 8
(5) $Hg + 3Cl^- \rightarrow HgCl_3^- + 2e^-$	$\frac{1}{2}\mu^*_{H_2} - \frac{1}{2}\mu^o_{Hg} - \frac{3}{2}RT \ln \lambda^\theta_{Cl^-} + \frac{1}{2}RT \ln \lambda^\theta_{HgCl_3^-}/(\lambda^\theta_{H^+})^2$	0·443 4
(6) $Hg + 4Cl^- \rightarrow HgCl_4^{2-} + 2e^-$	$\frac{1}{2}\mu^*_{H_2} - \frac{1}{2}\mu^o_{Hg} - 2RT \ln \lambda^\theta_{Cl^-} + \frac{1}{2}RT \ln \lambda^\theta_{HgCl_4^{2-}}/(\lambda^\theta_{H^+})^2$	0·413 8
(7) $Hg_2^{2+} + 6Cl^- \rightarrow 2HgCl_3^- + 2e^-$	$\frac{1}{2}\mu^*_{H_2} - \frac{1}{2}RT \ln \lambda^\theta_{Hg_2^{2+}}(\lambda^\theta_{H^+})^2 - RT \ln (\lambda^\theta_{Cl^-})^3/\lambda^\theta_{HgCl_3^-}$	0·097 87
(8) $Hg_2^{2+} + 8Cl^- \rightarrow 2HgCl_4^{2-} + 2e^-$	$\frac{1}{2}\mu^*_{H_2} - \frac{1}{2}RT \ln \lambda^\theta_{Hg_2^{2+}}(\lambda^\theta_{H^+})^2 - RT \ln (\lambda^\theta_{Cl^-})^4/\lambda^\theta_{HgCl_4^{2-}}$	0·038 52

$$\times \exp\left[\frac{2F}{RT}(U^{\theta}_{Hg_2^{2+}/HgCl_3^-} - U^{\theta}_{Hg/HgCl_3^-})\right]. \quad (25)$$

From entries 5 and 7 of Table 1,

$$c_{Hg_2^{2+}} = \frac{\rho_o^3 c_{HgCl_3^-}}{c_{Cl^-}^3}(2{\cdot}08 \times 10^{-12})\,\text{mol}\,l^{-1}, \quad (26)$$

and may therefore be neglected from further consideration. Preliminary data on this system have been obtained by the authors [17] in a porous carbon reactor. For a feed concentration of 4·12 mg l^{-1} of mercury, a value of $VOP_{max} = -0{\cdot}46$ V was found, with $c_{Cl^-} = 4{\cdot}35$ mol l^{-1} in the brine. Substituting these values into Equations 21 to 23 yields a total mercuric concentration of $1{\cdot}36 \times 10^{-14}$ mg l^{-1}, the complex $HgCl_4^{2-}$ predominating. Under these conditions Equation 25 or 26 yields the estimate of the mercurous dimer as $1{\cdot}52 \times 10^{-27}$ mg l^{-1}.

2.4. *Lead removal from lead–sulphate solutions*

A preliminary study has been made on this system by the authors [6]. An expression for the equilibrium lead ion concentration may be obtained by considering the working electrode reaction to be

$$Pb^{2+} + 2e^- \rightarrow Pb,\ U^{\theta}_{Pb/Pb^{2+}} = -0{\cdot}126\,V, \quad (27)$$

with the result

$$c_{Pb^{2+}} = \frac{\rho_o^3}{c^2_{Cl^-,sat}} \exp\left(\frac{2F}{RT}\Delta V_k\right). \quad (28)$$

For a feed concentration of lead of 4·32 mg l^{-1} a maximum operating potential VOP_{max} was found to be −0·56 V. Substituting this value into Equation 28 yields an equilibrium lead ion concentration of $c_{Pb^{2+}} = 1{\cdot}35 \times 10^{-7}$ mol l^{-1} or 0·028 mg l^{-1} of lead.

2.5. *Oxidation of ferrous ion*

Adams *et al.* [9] have studied ferrous oxidation on a porous carbon electrode from a dilute stream containing 1·43 g l^{-1} of H_2SO_4. On an inert carbon electrode, only the following redox reaction need be considered:

$$Fe^{2+} \rightarrow Fe^{3+} + e^-,\ U^{\theta} = 0{\cdot}771\,V, \quad (29)$$

where the equilibrium ferrous composition may be estimated from

$$c_{Fe^{2+}} = \frac{c_{Fe^{3+}} c_{Cl^-,sat}}{\rho_o} \exp\left(\frac{-F}{RT}\Delta V_k\right) \quad (30)$$

if the ferric composition is known. If the reactor is long enough, the reaction (Equation 29) will have gone to complete conversion except for the equilibrium composition exiting at a particular value of the operating potential. Thus, for a feed composition of 705 mg l^{-1} ferrous ion and a maximum value of the operating potential of $VOP_{max} = 0{\cdot}7$ V, the equilibrium ferrous concentration may be estimated to be $c_{Fe^{2+}} = 1{\cdot}4$ mg l^{-1}.

2.6. *Experimental minimum concentration*

The minimum wall concentration calculated in Sections 2.1–2.5 must be compared with the minimum bulk average concentration leaving the reactor because the equilibrium wall concentration is not easily measured. Table 2 lists the measured minimum bulk concentration obtained by various authors in porous flow-through electrode reactors. Also, shown are the predicted minimum wall concentrations for these systems which were calculated in Sections 2.1–2.5 for the experimental values listed in the table.

The experimental bulk concentration will approach the predicted wall concentration values if the reaction is carried to a greater degree of completion. This may be achieved by reducing the flow rate, while holding *VOP* constant, making the electrode thicker (upstream counter-electrode only), or adding additional reactors operating with equal values of *VOP*.

The discrepancies which exist between the predicted minimum wall concentration and the experimental bulk values may be explained as follows. For copper removal, the reactor was designed to operate with a mass-transfer limitation to remove copper from 667 to 1 mg l^{-1}, and not to remove all the copper. For mercury removal, the experimental minimum bulk concentration of less than 5×10^{-3} mg l^{-1} reported in Table 2 is due to the limitations of the analytical technique used for detecting mercury. For the operating potential reported, samples obtained from the dilute product stream of the reactor contained no detectable mercury. For ferrous oxidation only, the predicted minimum wall concentration is

Table 2. Experimental minimum bulk concentration and predicted minimum wall concentration for various systems

System	*Feed concentration* ($mg\ l^{-1}$)	*Observed effluent concentration* ($mg\ l^{-1}$)	*Electrode potential* (V)	*Calculated wall concentration* ($mg\ l^{-1}$)
Copper	667	0·06	−0·25	$4{\cdot}7 \times 10^{-5}$
Silver	1000	42	−0·46	23
Lead	4·32	0·55	−0·56	0·028
Mercury	4·12	< 0·005	−0·46	$1{\cdot}36 \times 10^{-14}$
Antimony	100	5	−0·3828*	$1{\cdot}62 \times 10^{-13}$
Ferrous oxidation	705	1	0·7	1·4

* Potential at which the calculated antimony wall concentration exhibits a minimum (see Fig. 3).

greater than the observed bulk value. Adams *et al.* [9] report that the current measured for this system is greater than that based on the feed composition ($i = nF\,v\,c_f$) at current efficiencies approaching 100%. One explanation presented by these authors is the oxidation of ferrous species by oxygen, a reaction which is catalysed on a graphite surface. For silver, the agreement is good; it should be noted that effluent values as low as $0{\cdot}8\ mg\ l^{-1}$ were achieved at *VOP* values as extreme as −0·55 V, but with a considerable loss of current efficiency due to side reactions.

3. The removal of antimony

As mentioned earlier, Kuhn and Houghton [7] have reported an apparent limit in the removal of antimony from aqueous solutions using a porous flow-through electrode reactor. Application of the criterion suggested in previous sections using the data of Kuhn and Houghton [7] is not possible since their study was one of transient response and no steady-state current–potential data were provided. However, qualitative information about their experiments allows a thermodynamic analy-

Table 3. Standard electrode potentials of antimony referred to the hydrogen electrode. Aqueous solutions at 25° C. Equilibrium wall concentration of antimony as a function of VOP

Reaction	U^θ (V)	*Concentration* ($mol\ l^{-1}$)
(1) $SbH_3 \rightarrow Sb + 3H^+ + 3e^-$	−0·5104	$c_{SbH_3} = \dfrac{(c_{H^+}c_{Cl^-,sat})^3}{\rho_0^5}\exp\left(-\dfrac{3F}{RT}\Delta V_k\right)$
(2) $2Sb + 3H_2O \rightarrow Sb_2O_3 + 6H^+ + 3e^-$	0·1445	$c_{Sb_2O_3} = \dfrac{\rho_0^{13}}{(c_{H^+}c_{Cl^-,sat})^3}\exp\left(\dfrac{6F}{RT}\Delta V_k\right)$
(3) $Sb + H_2O \rightarrow SbO^+ + 2H^+ + 3e^-$	0·2075	$c_{SbO^+} = \dfrac{\rho_0^6}{c_{H^+}^2 c_{Cl^-,sat}^3}\exp\left(\dfrac{3F}{RT}\Delta V_k\right)$
(4) $Sb + 3H_2O \rightarrow Sb(OH)_3 + 3H^+ + 3e^-$	0·2307	$c_{Sb(OH)_3} = \dfrac{\rho_0^7}{(c_{H^+}c_{Cl^-,sat})^3}\exp\left(\dfrac{3F}{RT}\Delta V_k\right)$
(5) $Sb + 2H_2O \rightarrow HSbO_2 + 3H^+ + 3e^-$	0·2309	$c_{HSbO_2} = \dfrac{\rho_0^7}{(c_{H^+}c_{Cl^-,sat})^3}\exp\left(\dfrac{3F}{RT}\Delta V_k\right)$
(6) $Sb + 2H_2O \rightarrow SbO_2^- + 4H^+ + 3e^-$	0·4633	$c_{SbO_2^-} = \dfrac{\rho_0^8}{c_{H^+}^4 c_{Cl^-,sat}^3}\exp\left(\dfrac{3F}{RT}\Delta V_k\right)$

sis to be undertaken which indicates that a minimum exists in the antimony concentration as a function of *VOP*.

3.1. *Analysis*

The chemistry of antimony in aqueous solutions is quite complex, and many molecular and ionic species are possible. Kuhn and Houghton [7] report that in their experiments the oxidation state of the dissolved antimony species was + 3. Table 3 lists the standard electrode potentials of various antimony species which are known to exist in the plus three oxidation state (values of which have been calculated from thermodynamic data [18] or found tabulated in the literature [19]). Stability data indicate that $Sb(OH)_3$, and SbO^+ are the most probable species and that Sb^{3+} rarely exists except under extremely acidic conditions [16]. Expressions for the equilibrium wall concentration as a function of *VOP* for each of the antimony species may be derived as before and are also given in Table 3.

3.2. *Results*

Fig. 3 depicts the dependence on *VOP* of the equilibrium wall concentration of the various antimony species found in Table 3, where the concentration of hydrogen ion has been set to 1 mol l^{-1}. The solid line represents the total equilibrium antimony concentration if all of these species are present in solution.

The minimum exhibited by the total antimony concentration is due to the evolution of stibine (SbH_3) in a minus three valence state at high cathodic potentials (negative values of *VOP*). This supposition is supported qualitatively by the data of Kuhn and Houghton [7], who report stibine evolution and low current efficiencies. The low current efficiencies are due to cell operation at cathodic potentials which are too high where both the evolution of stibine and hydrogen are appreciable. However, quantitatively the estimated equilibrium wall concentration (shown in Fig. 3) lies thirteen orders of magnitude below the reported bulk value. As discussed earlier, the bulk value will exceed the equilibrium value somewhat because of electrode-kinetic and mass-transfer limitations; however, a large discrepancy does exist. This may

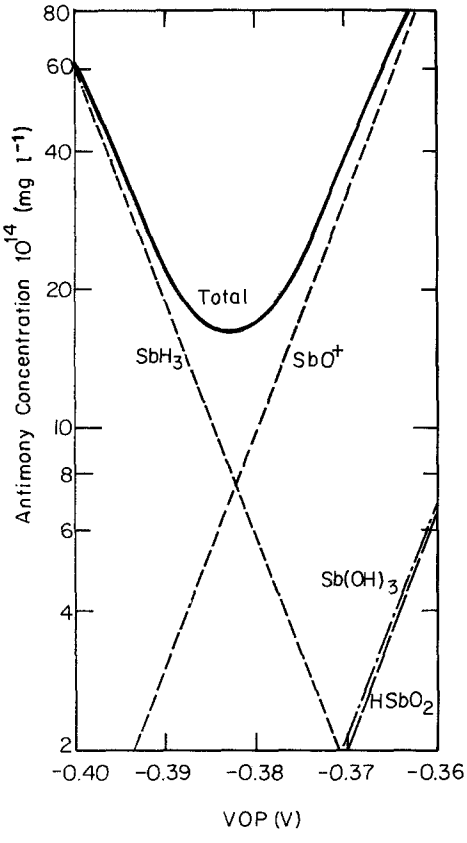

Fig. 3. Equilibrium antimony concentration as a function of electrode potential relative to a saturated calomel electrode.

be explained by considering the range of potential at which the predicted equilibrium wall concentration is less than or equal to the measured bulk value (5 mg l^{-1}). Calculations (using the expressions found in Table 3) indicate that this range of potential is $-0{\cdot}655 \leqslant VOP \leqslant -0{\cdot}130$ V. Since Kuhn and Houghton [7] operated their cell galvanostatically, their cell potential could vary over a wide range. To resolve the question of the practical lower limit attainable for antimony removal, careful, controlled-potential, steady-state experiments will be required.

4. General considerations

As discussed earlier, the bulk concentration of the reactant species will approach the equilibrium wall concentration predicted by thermodynamics if the reactor is made thicker (upstream counter-electrode only) or additional reactors are placed in

series. This may be seen quantitatively by considering the analysis presented by Bennion and Newman [1] for a reactor operating at the limiting current with an upstream counter-electrode (see [20] for the analysis of a downstream counter-electrode).

For reactions carried to a high degree of completion, the allowable potential variation across a reactor can be estimated approximately as

$$\Delta\Phi_2' \sim -\frac{nFv^2 c_f}{s_R a k_m \kappa}. \qquad (31)$$

This equation shows that the ohmic potential drop across a reactor is directly proportional to the feed concentration. In the copper recovery process of Bennion and Newman [1] a value of the operating potential *VOP* may be chosen to be $-0{\cdot}25$ V (the potential at the fluid outlet). If their reactor were operating at the design specification, $\Delta\Phi_2' = 0{\cdot}2$ V, the driving force at the front of the reactor would be $-0{\cdot}45$ V. The data indicate that the magnitude of this value does not produce appreciable side reactions – thus if this driving force could be maintained throughout the depth of the reactor the effluent concentration will ultimately be reduced. With this in mind, the ultimate value of *VOP* is then $-0{\cdot}45$ V. Equations 5 and 8 then yield an estimate of the lowest attainable equilibrium wall concentration for copper of $1{\cdot}94 \times 10^{-8}$ mg l^{-1}.

In order to achieve this in practice, consider reactors placed in series: if for example the concentration in the first reactor has been reduced by 99%, then the total current density in the second reactor ($i = nFvc_f$) will be smaller resulting in a reduction in the ohmic potential drop (see Equation 31), and the electrode potential can be maintained closer to $-0{\cdot}45$ V throughout the second reactor.

This also applies to short reactors where the reaction rate is non-zero at the back of the reactor resulting in an appreciable surface overpotential, thereby producing a wall concentration higher than the equilibrium value. Increasing the reactor thickness will also decrease the wall concentration toward the equilibrium value if the counter-electrode and current collector are placed upstream (or if the matrix conductivity is high) [20].

5. Conclusions

A criterion has been suggested for determining the minimum concentration attainable in a porous flow-through electrode reactor. This may be done by measuring the cell current as a function of the potential of the working electrode current collector relative to a reference electrode of a given kind placed in the effluent stream (see Fig. 1). Thermodynamics may then be applied by assuming that this measured potential can be set equal to an expression for the open-circuit cell potential between these electrodes, thereby yielding a value of the equilibrium wall concentration of the reactant species. It should be emphasized that the value of the minimum concentration obtained is a lower limit.

Comparison of this concentration with the experimentally observed effluent concentration suggests that the procedure is essentially correct, although the effluent concentration will be higher than that calculated if the reactor thickness is small and mass-transfer and electrode kinetic limitations still exist at the fluid outlet. If either mass transfer limitations or kinetic factors appear to be dominant, the reactor may well have been designed so that the effluent concentration can be predicted on the basis of these governing factors and an estimation based on thermodynamic considerations would not be necessary.

Measurement of the reactor operating potential as described above should help to clarify lower limits observed in flow-through electrochemical reactors. It should also aid in the design of reactor systems, since information on the allowable ohmic potential variation within the solution from the inlet to the outlet of the reactor is provided.

Acknowledgement

This report was done with support from the United States Energy Research and Development Administration. Any conclusions or opinions expressed in this report represent solely those of the authors and not necessarily those of The Regents of the University of California, the Lawrence Berkeley Laboratory or the United States Energy Research and Development Administration.

References

[1] D. N. Bennion and J. Newman, *J. Appl. Electrochem.* **2** (1972) 113.

[2] J. Van Zee and J. Newman, *J. Electrochem. Soc.* **124** (1977) 706.

[3] A. K. P. Chu, M. Fleischmann and G. J. Hills, *J. Appl. Electrochem.* **4** (1974) 323.

[4] A. T. Kuhn and R. W. Houghton, *Electrochim. Acta* **19** (1974) 733.

[5] G. Kreysa, S. Pionteck, E. Heitz, *J. Appl. Electrochem.* **5** (1975) 305.

[6] J. A. Trainham and J. Newman, *Inorganic Materials Research Division Annual Report* (1973), LBL-2299, Berkeley, Lawrence Berkeley Laboratory, University of California (1974).

[7] A. T. Kuhn and R. W. Houghton, *J. Appl. Electrochem.* **4** (1974) 67.

[8] J. Newman, 'Electrochemical Systems', Prentice-Hall, Englewood Cliffs, N. J. (1973), (a) chapters 2 and 3, (b) p. 57.

[9] G. B. Adams, R. P. Hollandsworth and D. N. Bennion, *J. Electrochem. Soc.* **122** (1975) 1043.

[10] J. A. Trainham and J. Newman, *J. Electrochem. Soc.* (in press).

[11] D. K. Roe, *Analyt. Chem.* **36** (1964) 2371.

[12] R. Alkire and P. K. Ng. *J. Electrochem. Soc.* **121** (1974) 95.

[13] J. R. Backhurst, J. M. Coulson, F. Goodridge, R. E. Plimley and M. Fleischmann, *ibid* **116** (1969) 1600.

[14] A. F. Trotman-Dickerson (ed.), 'Comprehensive Inorganic Chemistry', Vol. 3, (1973) p. 85.

[15] L. Meites, ed., 'Handbook of Analytical Chemistry', McGraw-Hill Book Company, New York (1962) p. 37.

[16] C. F. Baes, Jr., R. E. Mesmer, 'The Hydrolysis of Cations, A Critical Review of Hydrolytic Species and their Stability Constants in Aqueous Solutions', ORNL-NSF-EATC-3 Oak Ridge Nat'l Lab., Oak Ridge, TN 37830 (Dec. 1975).

[17] J. A. Trainham and J. Newman. Unpublished results (1975) Berkeley: University of California.

[18] D. D. Wagman, W. H. Evans, V. B. Parker, I. Halow, S. M. Bailey and R. H. Schumm, *Selected Values of Chemical Thermodynamic Properties. Tables for the First Thirty-Four Elements in the Standard Order of Arrangement*, NBS Technical Note 270-3. Washington, D. C., National Bureau of Standards (1968) p. 99.

[19] R. C. Weast, ed., 'Handbook of Chemistry and Physics', 51st Ed. Chemical Rubber Co., Cleveland, Ohio (1971).

[20] J. Newman and W. Tiedemann, *Adv. Electrochem. and Electrochem. Eng.* John Wiley and Sons, New York, (1977).